

# Single photoionization of Be and HF using the multiconfiguration time-dependent Hartree-Fock method

D. J. Haxton,<sup>1</sup> K. V. Lawler,<sup>1</sup> and C. W. McCurdy<sup>1,2</sup>

<sup>1</sup>*Chemical Sciences and Ultrafast X-Ray Science Laboratory, Lawrence Berkeley National Laboratory, Berkeley, California 94720, USA*

<sup>2</sup>*Department of Chemistry, University of California, Davis, Davis, California 95616, USA*

(Received 1 May 2012; published 10 July 2012)

A recently developed *ab initio* implementation of the multiconfiguration time-dependent Hartree Fock (MCTDHF) method is used to calculate valence and core photoionization cross sections of the Be atom and HF molecule in the Born-Oppenheimer approximation. The cross sections are extracted from the dynamics following excitation by a single subfemtosecond laser pulse. We compare with previously published results and those from time-independent complex Kohn scattering calculations and find that the MCTDHF method calculates both the magnitude of the cross section and the line shapes of the resonant peaks to good accuracy, particularly for valence photoionization. These calculations demonstrate a methodology immediately applicable to calculating multiphoton and ultrafast dynamics.

DOI: [10.1103/PhysRevA.86.013406](https://doi.org/10.1103/PhysRevA.86.013406)

PACS number(s): 32.80.Fb, 33.80.Eh, 31.15.xv

## I. INTRODUCTION

The multiconfiguration time-dependent Hartree-Fock (MCTDHF) method [1–18] has received considerable attention as a method for calculating electronically excited and nonlinear dynamics relevant to ultrafast experiments using ultraviolet and x-ray pulses. The ansatz of a time-dependent linear combination of time-dependent basis functions is a straightforward generalization of time-dependent configuration interaction (CI) and may be applied to any many-body quantum system. Known as the MCTDH method for systems without permutation symmetry, it has been fruitfully applied to problems of nuclear dynamics via the numerical implementation by Beck and co-workers [19,20], whose successful efforts include treatments of pyrazine including a conical intersection and with 24 degrees of freedom [21,22] as well as a full-dimensional calculation of the vibrational spectrum of  $\text{H}_5\text{O}_2^+$  [23–25] and that of malonaldehyde including tunneling splitting [26–28]. There are numerous other examples of successful calculations using the MCTDH method and MCTDH method version for bosons (MCTDHB) [29,30].

Despite the success of implementations of this idea for nuclear dynamics, dating back to the early 1990s [31], the application of the MCTDHF method to the electronic problem has proven more difficult. If the ionization continuum can be ignored, considerable progress can be made using the basis set methods of quantum chemistry [10–15], but treating the electronic continuum simultaneously with bound electronic motion requires considerably more effort. A one-dimensional treatment of photoionization with the MCTDHF method has been demonstrated in Refs. [3,4]. The  $\text{H}_2$  molecule has been treated in full dimensionality using grid methods in the MCTDHF method and an absorptive term in the Hamiltonian to eliminate the outgoing flux [8,9].

Without the ability to treat both the ionization continuum and correlated electron dynamics in full dimensionality for many-electron atoms and molecules, the MCTDHF idea cannot treat the dynamics of an entire generation of ultrafast experiments in which the energy distributions of

photoelectrons ejected by probe pulses is the key experimental observable that provides a window on both electronic and nuclear dynamics on their intrinsic time scales. It has therefore been essential to develop an implementation of the MCTDHF method that can treat photoionization accurately—including resonance phenomena—and that is the subject of this study.

We have developed an implementation of the MCTDHF approach for ultrafast and nonlinear dynamics in atoms and diatomic molecules, designed to overcome the main barriers to the calculation of an accurate solution of the electronic nonrelativistic time-dependent Schrödinger equation for a molecule subject to arbitrary laser pulses. The details of the method have been described at length previously [32].

(i) It represents the ionization continuum rigorously via the method of complex coordinate scaling [33–38].

(ii) It is an all-active-electron method in which excitations are allowed from all orbitals and all orbitals are time dependent.

(iii) It employs a sparse matrix representation of the Hamiltonian using a localized interpolating polynomial [discrete variable representation (DVR)] basis [39–41] implemented in finite elements [42,43]. In contrast to those among a Gaussian orbital basis, the two-electron matrix elements are extremely sparse, a property that is crucial for efficient time propagation. The DVR basis is built on a product grid of quadrature points.

(iv) It treats atomic problems in spherical polar coordinates and diatomics in prolate spheroidal coordinates.

(v) It efficiently and stably integrates the nonlinear, unitary, and stiff differential equations of motions of the coupled orbital and configuration coefficients via a generalization of the mean-field method of Beck *et al.* [20].

(vi) It includes a rigorous treatment of nonadiabatic dynamics in diatomics, though this capability is not employed in the calculations presented here.

In order to demonstrate the capabilities of this implementation of the MCTDHF method, we should begin by calculating first-order quantities. Here we apply the method to the calculation of photoionization cross sections of Be and

HF. A single subfemtosecond laser pulse is used to calculate the cross section over the entire range of photon energies. In the case of the molecular example we perform calculations at a fixed internuclear distance and thus the autoionizing resonances in this system result in many features in the cross section that are not averaged out or modified by nuclear motion. The results are compared with prior experiment and theory and to results calculated with the complex Kohn variational method [44–46], which for HF are also performed at a fixed internuclear separation and should exhibit the same resonance features as the MCTDHF calculations.

## II. THE MCTDHF METHOD

The MCTDHF ansatz describes the wave function as a time-dependent linear combination of Slater determinants comprised of time-dependent orbitals

$$|\Psi(t)\rangle = \sum_a A_a(t) |\vec{n}_a(t)\rangle \quad (1)$$

in which each determinant  $a$  is specified by the vector  $\vec{n}_a$  and is defined by

$$|\vec{n}_a(t)\rangle = \mathcal{A} [|\phi_{n_{a1}}(t)\rangle \cdots |\phi_{n_{aN}}(t)\rangle]. \quad (2)$$

The time-dependent orbitals  $|\phi_n(t)\rangle$  are spin restricted and expanded in the underlying DVR basis defined on an underlying spherical polar or prolate spheroidal grid as described in Ref. [32].

Calculating photoionization cross sections is a particularly difficult test of the MCTDHF method. The MCTDHF working equations are arrived at by application of the Dirac-Frenkel variational principle to the MCTDHF wave-function ansatz. The resulting equations minimize the norm of the error in the time derivative for all time. Because the proportion of the wave function that is ionized is small, most of the variational flexibility in the trial wave function is engaged in accurately describing the time dependence of the initial state. This argument raises the possibility that the results of a practical MCTDHF photoionization calculation would depend upon the nature of the applied pulse. However, as demonstrated in Ref. [32], the calculated photoionization cross sections are consistent (graphically indistinguishable) over a range of laser intensities, from approximately  $10^9$  W/cm<sup>2</sup> to at least  $10^{13}$  W/cm<sup>2</sup>, and over a wide range of pulse frequencies and durations. They are similarly converged with respect to the mean-field time step. We report results using only linearly polarized laser pulses in the length gauge. Results computed in the velocity gauge are indistinguishable, as expected given the fact that the stationary quantity in the Dirac-Frenkel variational principle  $\langle \Psi | i \partial / \partial t - H(t) | \Psi \rangle$  is invariant with respect to the gauge transformation, as long as the calculation is converged with respect to the primitive basis.

In Ref. [32] we demonstrated a method wherein we solve only for the change in the wave function due to the pulse and not the entire wave function including the initial state. It was very effective in reducing the number of orbitals required to calculate the photoionization cross section of H<sub>2</sub>, but presently suffers from numerical instability. This technique is not employed presently, but we expect that it would yield more accurate cross sections for these molecules with fewer

orbitals as well. In particular, our previous calculations on H<sub>2</sub> indicated that the method accurately reproduces ionization potentials with far fewer orbitals. The current results, however, permit an evaluation of the unelaborated MCTDHF method.

Full CI is employed within the electronic space and therefore the description of the calculations requires only the specification of the primitive basis and the number and symmetry labels ( $\sigma$ ,  $\pi_u$ ,  $p$ ,  $d$ , etc.) appropriate to the orbitals before the pulse is applied. For atoms or diatoms oriented parallel to the polarization direction, there is no loss of generality in restricting the electronic angular momentum number  $\mathcal{M}$  of each orbital. For diatoms not oriented parallel to the polarization direction, the  $\mathcal{M}$  quantum number is not restricted and a sum over all included  $\mathcal{M}$  values is included in the representation of each orbital, giving fully time-dependent three-dimensional orbitals. The representation in terms of the Slater determinants of these orbitals is periodically projected onto spin eigenfunctions in order to eliminate numerical contamination by other spin states.

We begin with a representation of the initial ground state including the most relevant (highest-occupied) natural orbitals. We propagate this wave function, applying a few-cycle pulse (0.5 fs in most of the applications here). Subsequent to the pulse we must propagate for 5–100 fs in order to accumulate the Fourier transforms for the cross-section calculation. The vast majority of the computational time is therefore spent after the pulse is finished. These long propagation times are at present necessary to resolve sharp features of the photoionization cross sections. For other applications, such as for transitions between bound states, these long propagation times would not be necessary. In practice, the calculations described here take 1–30 days on a single processor computer. The rate limiting step is the orbital propagation, not the propagation of the CI coefficients in Eq. (1).

The ionization continuum is represented using exterior complex scaling (ECS) [33–38]. This is a formally exact analytic technique that enforces outgoing boundary conditions on the wave function. It yields a non-Hermitian Hamiltonian with negative-definite imaginary part that absorbs outgoing flux in the asymptotic region. It permits a rigorous evaluation of cross sections via the method described in Ref. [32], which follows the implementation for complex absorbing potentials described in Ref. [47]. In the present calculations we include projection on final states of the cation in order to calculate partial cross sections (and therefore electron kinetic-energy distributions). The exact expression for the outgoing flux in cation channel  $\alpha$  at energy  $E$ ,  $f_\alpha(E)$ , is

$$f_\alpha(E) = \int_0^\infty dt \int_0^\infty dt' e^{iE(t'-t)} \times \langle \Psi(t) | \psi_\alpha \rangle [\psi_\alpha | i(\hat{H} - \hat{H}^\dagger) | \psi_\alpha] [\psi_\alpha | \Psi(t')], \quad (3)$$

where angular brackets denote integration over all  $N$  electrons and square brackets denote  $N - 1$ . We employ the approximation

$$[\psi_\alpha | i(\hat{H} - \hat{H}^\dagger) | \psi_\alpha] \approx \hat{Q} \equiv 2 \operatorname{Im} \left[ T_{\text{el}} + \begin{cases} \frac{1}{2|\vec{r}_N - \vec{R}_1|} + \frac{1}{2|\vec{r}_N - \vec{R}_2|} & \text{(diatom)} \\ \frac{1}{r_N} & \text{(atom)} \end{cases} \right], \quad (4)$$

where  $T_{el}$  is the kinetic-energy operator for the  $N$ th electron. The non-Hermiticity of the Hamiltonian results only from its representation on the ECS grid and arises primarily from the kinetic energy. This approximation provides a small correction due to the long-range Coulomb potential experienced by the outgoing electron without involving the coordinates of all the other electrons.

We therefore calculate the Dyson orbitals  $\chi_\alpha(t)$

$$\chi_\alpha(t) = \int d\vec{q}_1 \cdots d\vec{q}_{N-1} \psi_\alpha(\vec{q}_1 \cdots \vec{q}_{N-1})^* \Psi(t)(\vec{q}_1 \cdots \vec{q}_N) \quad (5)$$

by biorthogonalizing the orbitals as in Ref. [32] and calculate the flux via

$$f_\alpha(E) = \int_0^\infty dt \int_0^\infty dt' e^{iE(t'-t)} \langle \chi_\alpha(t) | \hat{Q} | \chi_\alpha(t') \rangle. \quad (6)$$

In tests of this method, it compared with the exact result to within three or four figures and is much faster. Whereas the flux calculations without approximation (total and projected) may take over a week on a single processor, the projected flux calculations using the above approximation require about an hour at most. The rate limiting step in either case is the biorthogonalization required to construct matrix elements or Dyson orbitals.

### III. VALENCE AND CORE PHOTOIONIZATION OF BERYLLIUM

#### A. Valence photoionization

Valence photoionization of beryllium has been the subject of many studies, both computational [48–63] and experimental [64–66]. The threshold for photoionization into the ground  $\text{Be}^+$  ( $1s^2 2s^2 S$ ) cation channel is 9.32 eV; the  $2p^2 P$ ,  $3s^2 S$ ,  $3p^2 P$ ,  $3d^2 D$ , and  $4s^2 S$  channels open at 13.28, 20.26, 21.28, 21.48, and 23.68 eV, respectively, and each supports a Rydberg series that contributes a dense series of peaks to the photoionization cross section.

Results are shown as calculated with three, six, and ten orbitals. We start with three orbitals, all initially  $s$  orbitals before the pulse; for the six-orbital calculations a  $p$  shell is added; for ten an additional  $s$  orbital and  $p$  shell are added. These calculations have 9, 81, and 651 Slater determinants and a singlet configuration space of dimension 6, 37, and 259, respectively. The pulse waveform is shown in Fig. 1 together with its spectral density. We use an angular DVR grid of five

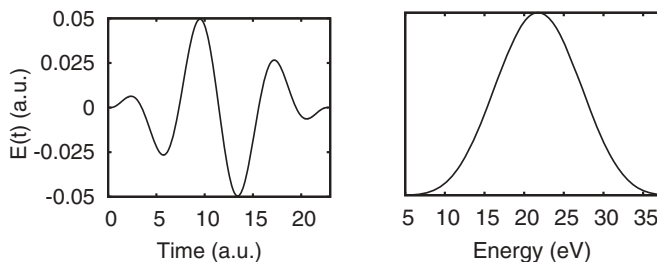


FIG. 1. Pulse used in Be valence photoionization calculations: left, pulse waveform; right, spectral density. The intensity is  $10^{14} \text{ W cm}^{-2}$ .

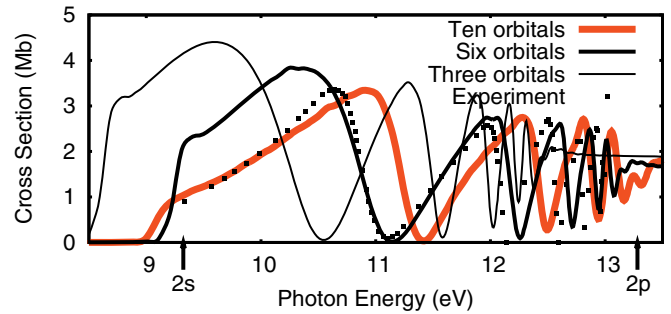


FIG. 2. (Color online) Beryllium valence photoionization cross section below the  $2p$  cation threshold calculated with ten, six, and three orbitals as described in the text and the experimental results of Ref. [64], as digitized from that reference. The experimental values for the  $2s$  and  $2p$  ionization thresholds are marked with arrows.

points in  $\theta$  and a radial grid with fifteen grid points per finite element. We use sixteen finite elements, the first of length  $1.5a_0$  providing a dense grid to represent the  $1s$  orbital and orbital cusps, the subsequent twelve of length  $8a_0$ , and three final elements of length  $16a_0$ ,  $32a_0$ , and  $64a_0$ . Exterior complex scaling is applied starting at the twelfth element, with a scaling angle of 0.25 rad. To accumulate the Fourier transform the wave function is propagated for 2000 a.u. after the pulse (approximately 50 fs), except for the ten-orbital calculation, for which it is propagated for 1400 a.u.

The computed cross sections below the second ionization threshold,  $2p$ , into the ground  $2s$  channel of the  $\text{Be}^+$  ion display the first members of the autoionizing series converging to that threshold. The results in this energy region are compared with the experimental results of Ref. [64] in Fig. 2. The three-orbital results yield effective thresholds significantly displaced from their proper energies, while the six- and ten-orbital results reproduce the cation thresholds well. The first ionization potentials calculated directly by obtaining the ground and cation ground states via imaginary time relaxation are 9.21, 9.70, and 8.23 eV for the ten-, six-, and three-orbital treatments, respectively, compared with the experimental value of 9.32 eV. The errors in these ionization potentials are reflected in the apparent thresholds in Fig. 2, but in every calculation the series of autoionizing resonances is reproduced with similar widths and line shapes. The convergence of the photoionization cross section with respect to the total time of propagation is shown in Fig. 3. As would be expected, long propagation times are required to resolve higher members

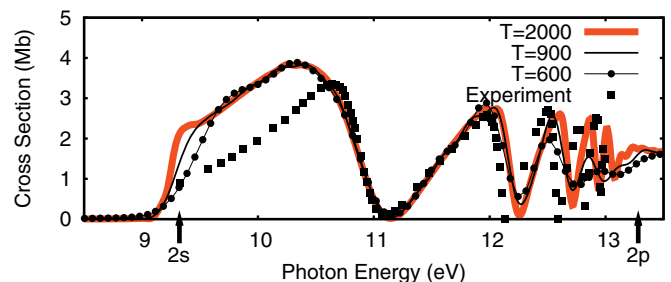


FIG. 3. (Color online) Convergence of the six-orbital beryllium valence photoionization cross section with respect to the total time of propagation, in a.u.

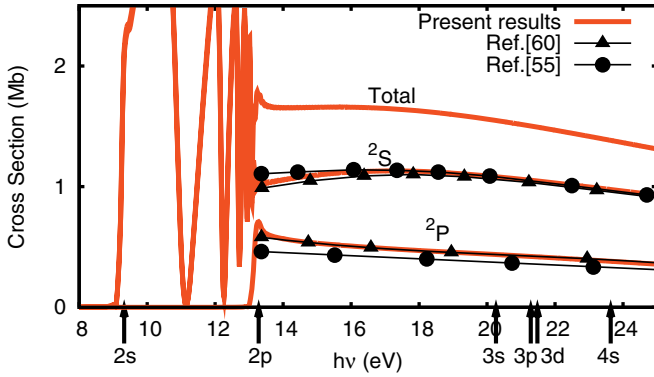


FIG. 4. (Color online) Excitation photoionization cross sections of beryllium calculated with six orbitals, compared with the random-phase approximation and Tamm-Dancoff theoretical results of Refs. [55,60].

of the Rydberg autoionizing series converging to the second threshold.

Results are shown for excitation photoionization using six orbitals in Fig. 4 and for total photoionization using ten orbitals in Fig. 5. The Rydberg series converging to the thresholds above the first,  $2s^2S$ , are not reproduced in the MCTDHF calculations; more orbitals are clearly required within the conventional MCTDHF framework. However, as shown in Fig. 4, the results obtained above the  $2p^2P$  threshold agree well with the multiconfiguration random-phase and Tamm-Dancoff approximations of Refs. [55,60], respectively. As shown in Fig. 5, the ten-orbital calculation produces features between the  $3s^2S$  and  $4s^2S$  thresholds reminiscent of Rydberg series, but these features are not converged.

### B. Core photoionization

Core ( $1s$ ) photoionization of beryllium has been studied both computationally [67–71] and experimentally [72–74]. We study it here using three, six, seven, and ten orbitals, again performing full configuration interaction in all calculations. The seven-orbital treatment has an additional  $s$  orbital relative to that with six orbitals, but otherwise is the same as the valence calculations; the seven-orbital calculation has 171 Slater determinants and a singlet space of dimension 76. We use an angular grid of five points in  $\theta$  and a radial grid with fifteen grid points per finite element. We employ sixteen

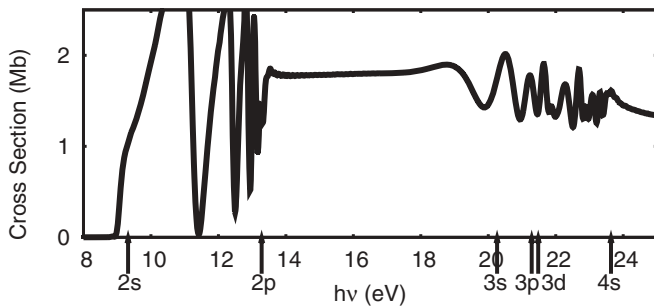


FIG. 5. Beryllium valence photoionization total cross section calculated with ten orbitals. The experimental values for the cation thresholds are marked with arrows.

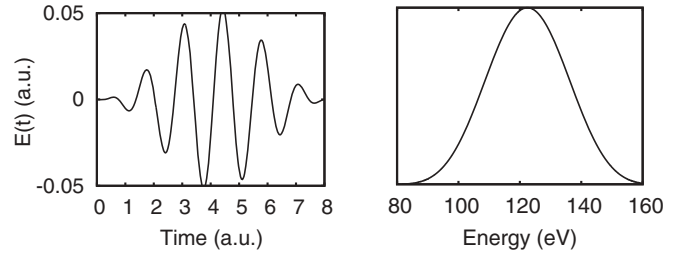


FIG. 6. Pulse used in Be core photoionization calculations: left, pulse waveform; right, spectral density. The intensity is  $10^{14}$  W cm $^{-2}$ .

elements with the first  $1.5a_0$  long, the next twelve  $6a_0$  long, then one each  $12a_0$ ,  $24a_0$ , and  $48a_0$  long, with complex scaling starting at the twelfth element at an angle of 0.25 rad. In each case the cross sections were extracted from the single pulse shown in Fig. 6. To accumulate the Fourier transform the wave function was propagated for 1400 a.u. (approximately 35 fs) and additionally for 4000 a.u. for the six-orbital calculation, after the pulse.

In Fig. 7 results are shown for core hole photoionization with three, six, seven, and ten orbitals. It is clear that the cross section has not converged with ten orbitals, but that nonetheless the calculation is successful in reproducing the basic features of the cross section. Literature values for the locations of the  $1s^12s^22p$  and  $1s^12s^23p^1P$  autoionizing states and of the  $1s^12s^22SK$  edge are marked in the figure and lie at 115.47, 121.40, and 123.63 eV, respectively [75]. These three features are reproduced in the calculated cross sections, though their locations are only correct to within a few eV.

All the calculations shown in Fig. 7 reproduce the prominent peak corresponding to the  $1s \rightarrow 2p$  autoionizing state, with the larger calculations obtaining its location to within approximately 1 eV; the calculations yield a  $K$  edge at approximately 127 eV, more than 3.5 eV above the physical threshold. For the three- and six-orbital calculations, the cross section otherwise consists of a sharp edge and monotonically decreasing and featureless result above it. The seven- and ten-orbital calculations include enough variational flexibility to reproduce the  $1s^{-1}3p$  peak below the  $K$  edge, though its energy is similarly approximately 3.5 eV too high. The inclusion of another initial  $s$  orbital, in the seven-orbital calculation, alters the result above the edge dramatically, building in a minimum in the cross section around 132 eV. Results from an eleven-orbital calculation with an additional

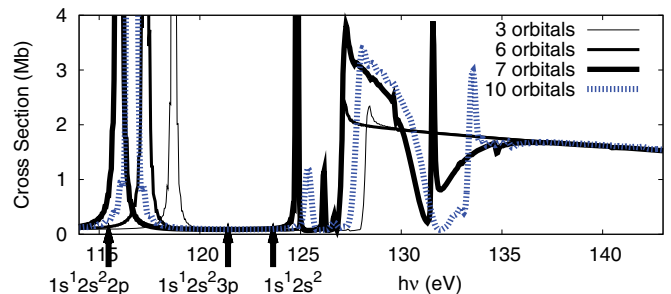


FIG. 7. (Color online) Beryllium core hole photoionization result for three, six, seven, and ten orbitals as described in the text.

$s$  orbital are not shown and were very close to the ten-orbital results.

The results with ten orbitals are compared with the experiment of Jannitti *et al.* [72] and the calculation of VoKy *et al.* [67] in Fig. 8. In the left panel the calculation is compared with the experiment. There is a fortuitous exact agreement in the location of the prominent  $1s^{-1}2s^22p^1P$  autoionizing resonance. Otherwise there is little agreement between the calculation and the experiment, except in the magnitude in the featureless region, which is reproduced accurately. In the right panel, the calculation is shown relative to the prior theory, shifted such that the  $K$  edge agrees with the literature value. Shifting the MCTDHF result makes the agreement in the  $1s^{-1}2p$  peak location worse, but shows the correspondence between the prominent minimum calculated presently and the thick forest of resonance peaks in the prior calculation in the region of 126–129 eV and accurately reproduces the position of  $1s^{-1}3p$ . The experiment of Jannitti *et al.* [72] does indicate that there is a drop in the cross section at approximately 125–126 eV.

### C. Auger decay

The resonance peaks in the core hole photoionization spectrum below the  $1s^{-1}$  edge, seen for instance in Fig. 8, correspond to metastable electronic states of the neutral that emit the photoelectron via Auger decay, a two-electron transition in which the  $1s$  orbital is filled. It is not immediately obvious that the MCTDHF wave function can accurately describe this decay. Nonetheless, a Breit-Wigner fit of the  $1s^{-1}2p$  resonance yields a width of 35.6 meV for the six-orbital calculation (which was propagated to 100 fs, enabling the fit). This result compares well with a prior theoretical result of 37 meV [76] and to an experimental result of 33–38 meV (1.2 or 1.4 mhartree) [77], confirming that the MCTDHF method accurately describes this process.

## IV. PHOTOIONIZATION OF THE HF MOLECULE

We calculate photoionization of the HF molecule using a bond length of  $1.733a_0$ . To assess the accuracy of these fixed-nuclei calculations, the details of which are not directly comparable to experiment due to nuclear motion, the calculated MCTDHF cross sections are compared with those calculated using the complex Kohn method [44–46]. These are two completely different approaches to the calculation of photoionization cross sections. The complex Kohn method employs a variational principle for the  $T$  matrix and a single-particle basis of Gaussians and numerical continuum functions, in which the  $N$ -electron scattering wave function is expanded via close coupling among explicit (approximate)  $(N - 1)$ -electron cation states. The MCTDHF method treats both the  $N$ - and  $(N - 1)$ -electron states implicitly in the expansion in Eq. (1).

Agreement between these two approaches is strong evidence of the accuracy of both. The reproduction of narrow autoionizing features in the photoionization cross section is a particularly stringent test of the MCTDHF method since those features must be computed via the Fourier transform of

TABLE I. Gaussian exponents of the scattering orbital basis used for complex Kohn scattering calculations obtained via the method of Ref. [78], which are capable of describing He Rydberg states to within a few wave numbers up to  $n = 4$ .

$\alpha_s$	$\alpha_p$	$\alpha_d$
1.05355602	1.58024691	0.500000000
0.341506727	0.266825024	0.098765432
0.098765432	0.098765432	0.031250000
0.031250000	0.044582625	0.012800000
0.012800000	0.022549196	0.006172839
0.006172839	0.012800000	0.002528395
0.002528395	0.006172839	0.002528395

the results of long propagations of the time-dependent wave function.

## A. Computational methodology

### 1. Complex Kohn scattering calculations

In order to reproduce the Rydberg series converging to excited cation thresholds in the complex Kohn calculation, we include a scattering orbital basis that was constructed with the method of Ref. [78] to accurately represent Rydberg states of helium to within a few wave numbers up to  $n = 4$ . The exponents used for the uncontracted functions are listed in Table I. Partial wave scattering channels up to  $l = 2$  are included.

The scattering basis specified above is combined with Dunning’s aug-cc-pVTZ basis [79] to make the single-particle Gaussian basis of the complex Kohn calculation. The Dunning basis is modified by removing the  $d$  and  $f$  orbitals from the hydrogen and fluorine centers, uncontracting the hydrogen  $s$  functions, and adding to fluorine two  $s$  functions with exponents 24 and 8 and two sets of  $p$  functions with exponents 25 and 9. This gives basis sets of size  $[6s, 3p]$  and  $[7s, 6p, 3d]$  for hydrogen and fluorine, respectively.

The apparent channel thresholds calculated within the MCTDHF method are in error by fractions of an eV. The complex Kohn scattering calculation requires careful balancing of the molecular orbital basis, which must represent both the neutral initial state and the cation final states, to produce accurate channel thresholds. To facilitate comparison, the orbital basis used in the complex Kohn calculation is tuned such that the channel thresholds agree with those in the MCTDHF calculation. This task is performed by using a state-averaged multiconfiguration self-consistent field (MCSCF) calculation in which the molecular orbitals minimize the weighted average energy of the ground neutral initial state and the  $N$ -included cation states. The  $N$ -independent weight fractions are determined by requiring the  $N$  channel thresholds to match. For the MCSCF we employ the Columbus quantum chemistry suite [80–84].

### 2. The finite-element DVR basis in prolate spheroidal coordinates for MCTDHF calculations

The primitive interpolating polynomial bases employed in the MCTDHF calculations are quite widely spaced. We find that the photoionization results are converged to graphical

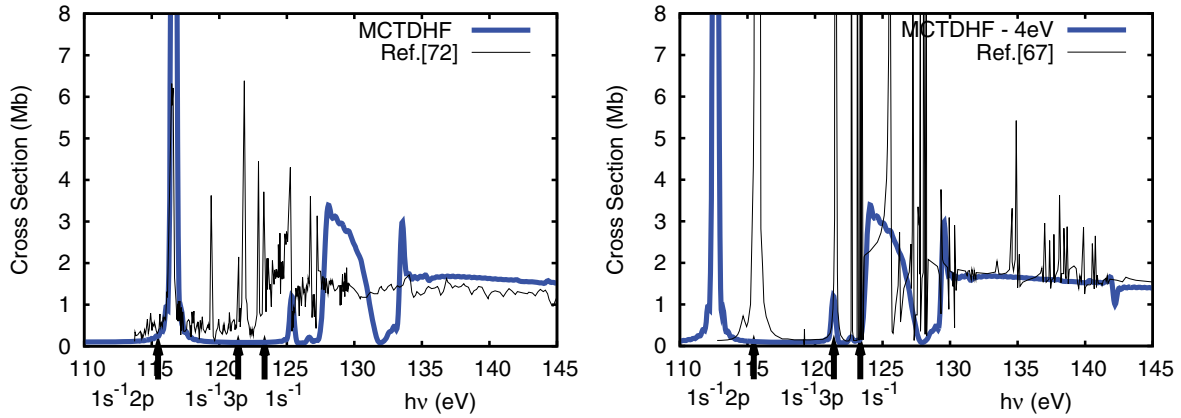


FIG. 8. (Color online) Comparison of the calculated beryllium core hole photoionization cross section with ten orbitals with the theoretical results of Ref. [67] (right) and the experimental results of Ref. [72] (left). The comparison with theory is shown shifted by 4 eV to make the apparent  $K$  edge correspond to the literature value of 123.35 eV.

accuracy with a primitive basis for which the energy of the ground state is not converged (but for which the excitation energies are converged). The product DVR basis is implemented in finite elements in the prolate spheroidal coordinates,  $1 \leq \xi \leq \xi_{\max}$  and  $-1 \leq \eta \leq 1$  multiplied by  $\exp(i\mathcal{M}\phi)$  for the dependence on the azimuthal angle. The calculations on HF use a DVR basis with eight points in a single element in  $\eta$ . We use 15 finite elements in  $\xi$ , the first of size 2, twelve of 8, and one each of 16 and 32 with 15 DVR grid points per element and with exterior complex scaling starting at the ninth element (at  $\xi = 59$ ). The first five elements are used in the calculation of the ground state. The maximum value of  $|\mathcal{M}|$ ,  $\mathcal{M}_{\max}$ , is 1 and 2 for parallel and perpendicular polarization calculations, respectively. This basis gives an eight-orbital ground-state energy of  $-99.778$  hartree. In comparison, with 15 points in  $\eta$  and 21 per element in  $\xi$  the energy of the eight-orbital ground state is  $-100.172$  hartree.

### B. The MCTDHF calculations of valence photoionization

We performed MCTDHF calculations on valence photoionization of HF using nine orbitals including one  $\pi$  and two  $\sigma$  in addition to the five occupied Hartree-Fock orbitals, with a full CI among the orbitals, giving 15 876 Slater determinants representing 5292 singlet spin adapted configurations in perpendicular polarization or 824 representing 296 with parallel polarization. We employ the pulse in Fig. 9. The wave

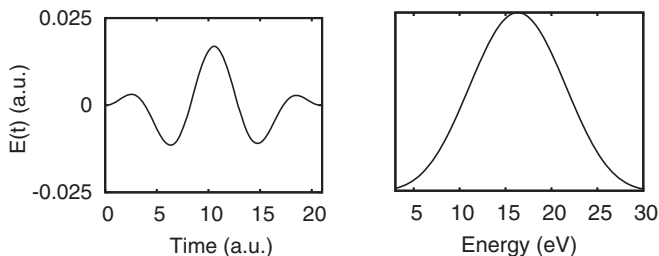


FIG. 9. Pulse used in HF valence photoionization calculations: left, pulse waveform; right, spectral density. The intensity is  $10^{13} \text{ W cm}^{-2}$ .

function is propagated for 2000 a.u. subsequent to the pulse to accumulate the Fourier transform.

In Fig. 10 the present results are compared with those from a complex Kohn scattering calculation with nine orbitals. For this calculation we define a reference space in which the  $1\sigma$  and  $2\sigma$  orbitals are doubly occupied and the remaining electrons are distributed among six orbitals. This yields 175 and 210 configurations for the ground and cation electronic states (spatial symmetry is not used to reduce the number of configurations). To obtain the orbitals MCSCF weights of 14 and 1 are used for the ground neutral and the  $^2\Sigma$  cation states, respectively. In the combined aug-cc-pVTZ and scattering orbital Gaussian basis, this yields corresponding energies of  $-100.1581$ ,  $-99.5636$ , and  $-99.4089$  hartree and ionization potentials of 16.177 and 20.385 eV, which are the channel thresholds in the complex Kohn calculation. These may be compared with experimental thresholds of 16.12 and 19.89 eV [85]. The complex Kohn calculation is not converged with respect to the primitive basis below approximately 17.5 eV.

In Fig. 10 we see that below the  $^2\Sigma$  cation threshold, the agreement between the calculations is remarkable, especially with parallel polarization. The Fano line shapes of the resonances and the magnitude of the cross section are in very close agreement. Above the  $^2\Sigma$  threshold, the magnitude of the  $^2\Pi$  cross section is larger in the MCTDHF calculation in parallel polarization and that of the  $^2\Sigma$  is larger in perpendicular polarization, but otherwise the magnitudes agree.

We also performed an eight-orbital MCTDHF calculation (one fewer than above) and a nine-orbital complex Kohn scattering calculation including fewer configurations than in the eight-orbital complex Kohn calculation above, which are not shown. The agreement in the line shapes of the  $^2\Pi$  Rydberg series (seen with perpendicular polarization) are better using the nine-orbital MCTDHF calculation above than that with eight orbitals. In contrast, the  $^2\Sigma$  resonance line shapes are converged with eight MCTDHF orbitals. The ninth MCTDHF orbital also has the effect of lowering the apparent threshold of the  $^2\Sigma$  channel in the MCTDHF calculation. With eight orbitals it is approximately 0.4 eV higher. The nine-orbital complex Kohn calculation with fewer configurations than the eight-orbital one produced a parallel polarization cross

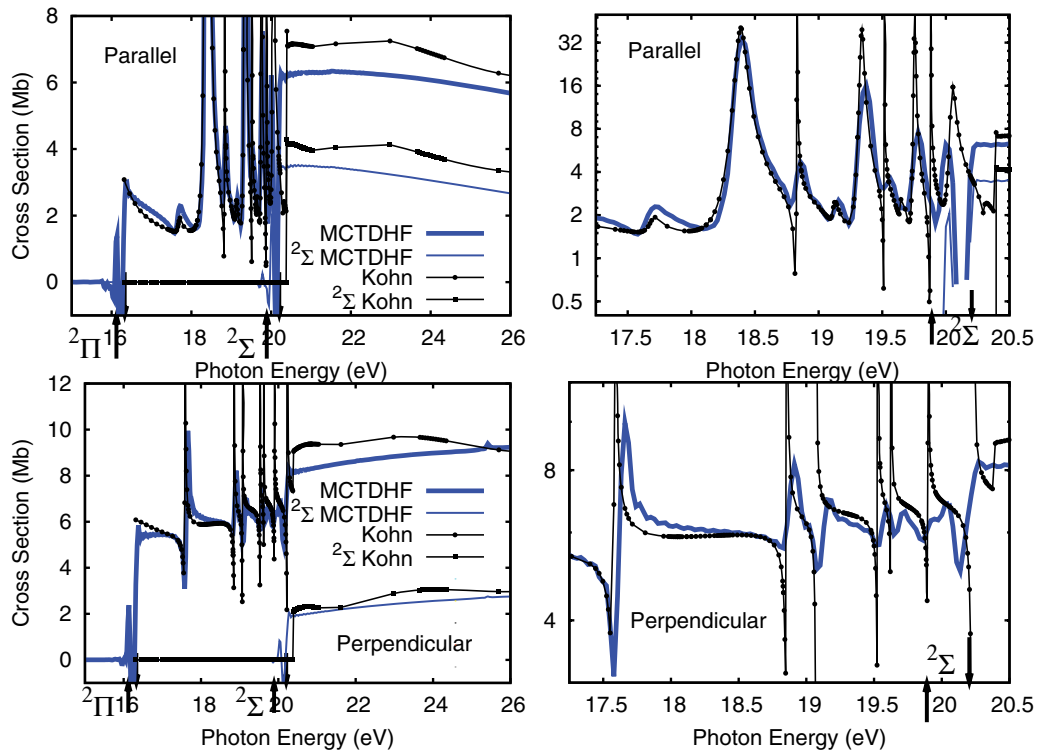


FIG. 10. (Color online) The HF photoionization calculated with nine orbitals compared with complex Kohn scattering results with eight orbitals, as described in the text. The experimental channel thresholds are marked with upward pointing arrows and the thresholds obtained using MCTDHF eigenfunctions for neutral and cation states with the same orbital basis are marked with downward pointing arrows.

section below the  $2\Sigma$  threshold significantly lower than that obtained from the other calculations. Of all these calculations the closest comparison between MCTDHF and complex Kohn calculations of the photoionization cross sections is that shown in Fig. 10.

### C. The $2\sigma$ photoionization

Inner-shell photoionization of the HF  $2\sigma$  orbital has been studied previously both theoretically [86,87] and experimentally [88]. To calculate photoionization in the vicinity of the  $2\sigma^{-1}$  ( $B^2\Sigma$ ) state the same primitive basis as for the valence photoionization calculations above was used, with nine orbitals, and the pulse shown in Fig. 11. For the complex Kohn scattering calculation the reference space includes all single, double, and triple excitations from the Hartree-Fock reference, with nine orbitals, yielding 470 configurations for

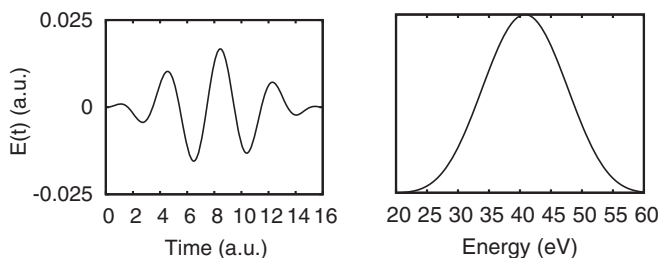


FIG. 11. Pulse used in the HF  $2\sigma$  photoionization calculations: left, pulse waveform; right, spectral density. The intensity is  $10^{13}$  W cm $^{-2}$ .

the cation and 466 for the neutral. The orbitals are optimized in a MCSCF calculation in which the neutral and the cation  $1\pi^{-1}$  ( $X^2\Pi$ ),  $3\sigma^{-1}$  ( $A^2\Sigma$ ), and  $2\sigma^{-1}$  ( $B^2\Sigma$ ) states have weights 100, 1, 1, 7, and 2. This calculation yields channel thresholds of 16.18, 20.03, and 41.2 eV, the latter of which may be compared with a prior theoretical result of approximately 39 eV [86]. We were not able to adjust the orbitals of the complex Kohn calculation to match the apparent threshold in the MCTDHF calculation, which is too high, located at 42 eV and therefore, in this case only, adjust the complex Kohn results by shifting them 0.54 eV upward in energy.

The MCTDHF and complex Kohn scattering results are compared in Fig. 12. The locations of the resonance peaks are generally very well reproduced, as are some of the line shapes. The partial cross sections into the  $3\sigma^{-1}$  state are in very good agreement, while for the  $1\pi^{-1}$  state there are significant but offsetting differences between the calculations in the perpendicular and parallel photoionization cross sections such that the total cross section averaged over orientations is in good agreement. The cross sections to the  $2\sigma^{-1}$  final state are in very good agreement, considering the small branching ratio into this channel.

We examine the resonance at 36 eV,  $2\sigma^{-1}4\sigma^1\Sigma$ , which is well isolated and broad. The peak total cross section is 6.82 and 6.61 Mb and the resonance widths are 0.170 and 0.244 eV for the MCTDHF and complex Kohn calculations, respectively. The background cross section is higher in the MCTDHF calculation. The MCTDHF resonance peak is nearly symmetric while the complex Kohn calculation has a Fano asymmetry parameter of  $-7.07$ . For the MCTDHF

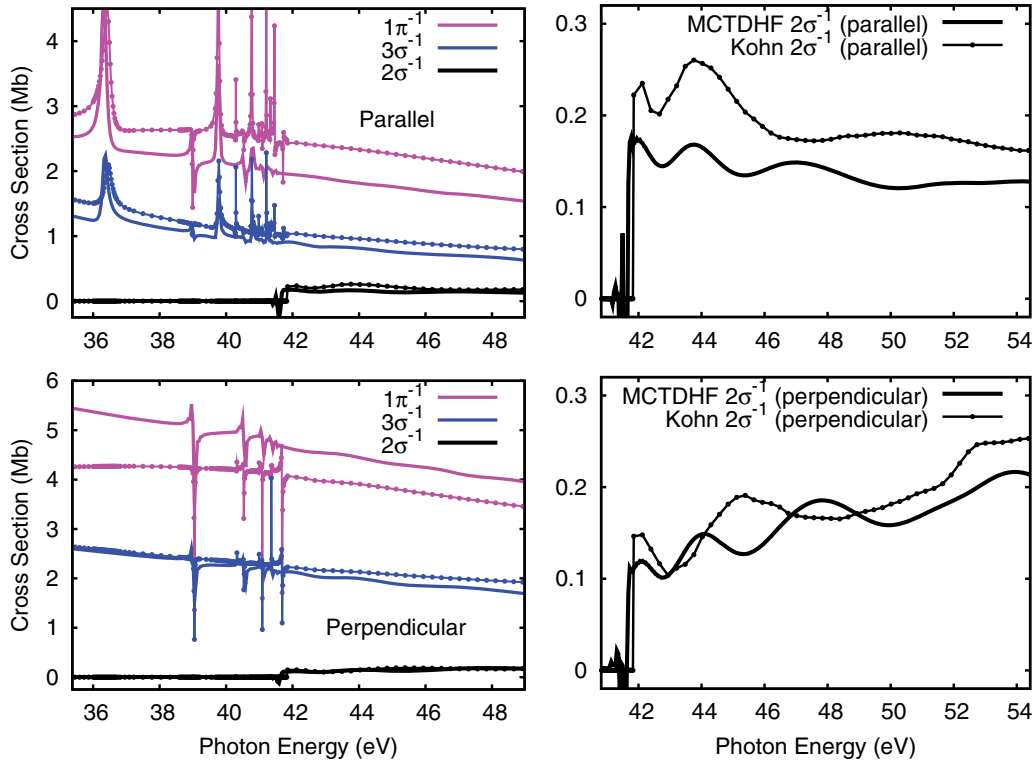


FIG. 12. (Color online) The HF partial photoionization cross sections near the  $2\sigma^{-1}$  ( $B^2\Sigma$ ) threshold: top row, parallel polarization; bottom row, perpendicular polarization with magnification of threshold region on right. In the left figures the cross sections for  $2\sigma^{-1}$ ,  $1\pi^{-1}$ , and  $3\sigma^{-1}$  increase in that order. Connected dots are complex Kohn scattering results; solid lines are MCTDHF results. The Kohn scattering results have been shifted by 0.54 eV.

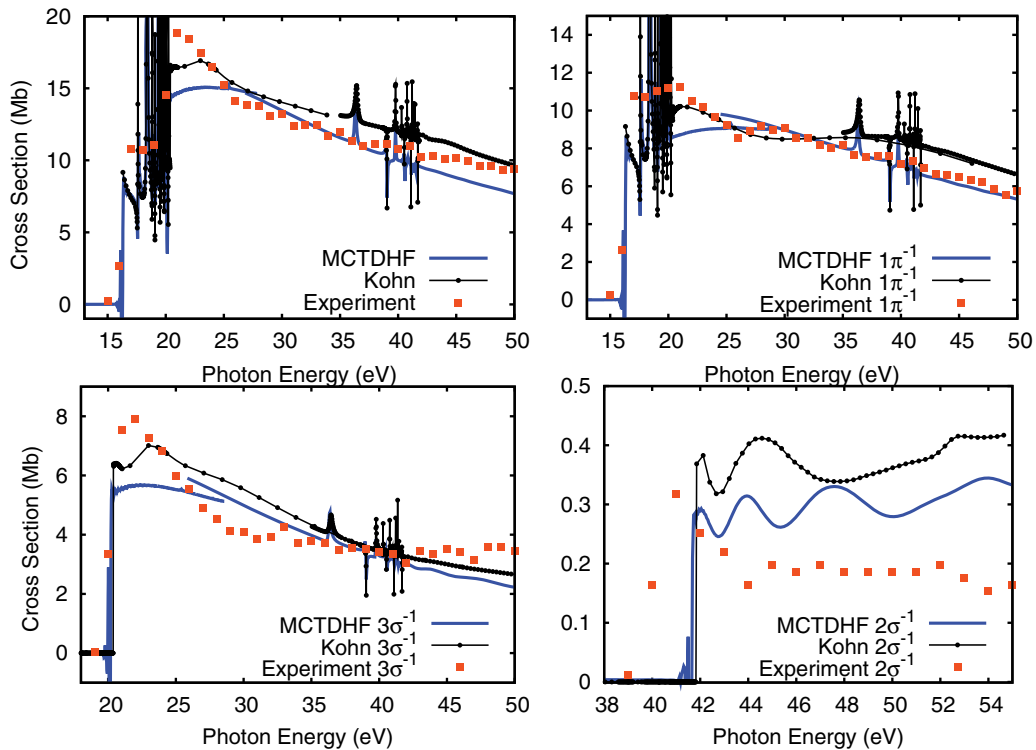


FIG. 13. (Color online) Comparison of MCTDHF and complex Kohn scattering results on total photoionization of HF (randomly oriented, perpendicular and parallel) both without respect to the final state (top left) and resolved into each final cation state (other panels) compared with those of the experiment of Brion and Thomson [89]. Two MCTDHF calculations, with pulses centered at high and low energy, are plotted.

calculation we obtain partial widths for the decay into the  $1\pi^{-1}$  ( $X^2\Pi$ ) and  $3\sigma^{-1}$  ( $A^2\Sigma$ ) cation channels in the ratio 1:0.437, while the ratio of the continuum background in the two channels is 1:0.523. The complex Kohn calculation gives the ratios 1:0.361 and 1:0.530, respectively, for those quantities. Thus we see that while there is significant disagreement in the widths, the magnitude of the cross sections, and the resonance branching ratio, the ratio of the continuum background in the two channels produced by the two calculations is in close agreement.

#### D. Comparison to experiment

In Fig. 13 the total cross sections (averaged over orientations, perpendicular and parallel polarization) for HF photoionization calculated with the MCTDHF method and the complex Kohn scattering method are presented and compared with the experiment of Ref. [89]. The comparison with experiment is quite favorable. The top left panel shows the total photoionization cross section. Both complex Kohn and MCTDHF calculations are in good agreement with experiment, but at higher energy it appears that the MCTDHF calculation agrees better with the experiment, the complex Kohn result being slightly too large. At low energy, the Born-Oppenheimer results differ qualitatively from the experimental result due to the thick series of Rydberg resonance peaks. In addition, the  $1\pi^{-1}$  and  $3\sigma^{-1}$  experimental cross sections are higher just above the latter threshold. However, the overall step in the cross section due to the opening of the  $3\sigma^{-1}$  channel is well reproduced. The magnitudes of the cross sections into the minor  $2\sigma^{-1}$  channel calculated by the two methods are in good agreement with each other and significantly above the experimental result.

#### V. CONCLUSION

The calculations presented here demonstrate that the implementation of the MCTDHF method originally described in Ref. [32] can be used to calculate photoionization cross sections for many-electron systems accurately. The calculations on hydrogen fluoride, with 30 quantum mechanical electronic degrees of freedom, indicate that the MCTDHF method for electrons may live up to the expectations following the success of the MCTDH method [19] for vibrational degrees of freedom. Details of the cross sections are reproduced

including the precise locations of and many if not all of the line shapes of autoionizing resonances.

These developments open the door for the application of this methodology to the accurate description of the coming generation of nonlinear ultrafast experiments, for instance, those using short UV and x-ray pulses as both a pump and probe. In such experiments all the valence electrons are active and may be excited or ionized, so simplified single-active-electron approximations are simply insufficient to describe the physics. The MCTDHF method provides an *all-electrons-active* description. A critical part of the capability demonstrated here is the projected flux formalism described in Eqs. (3)–(6) that allows the calculation of the photoelectron spectrum produced by a particular pulse sequence. Such quantities are the direct observable in ultrafast experiments and there is a crucial need for *ab initio* predictions with which to interpret those experiments.

There is still considerable room for improving the numerical robustness of MCTDHF calculations that include ionization. We anticipate that the convergence will improve with a numerically stable implementation of the method for calculating only the change in the wave function due to a radiation pulse that we described and demonstrated for photoionization of  $H_2$  in Ref. [32]. Other improvements would aim to increase the number of orbitals that may be tractably included in a MCTDHF calculation via the implementation of frozen orbitals and restricted configuration spaces or alternatively via methods used in nuclear shell model calculations [90] and recently developed for the MCTDH, MCTDHB, and MCTDHF methods [91–93] that may handle large numbers of configurations with full configuration interaction. The results presented here also open the way for the calculation of photoionization including nuclear motion in the MCTDHF method as previously described [32].

#### ACKNOWLEDGMENTS

Work performed at Lawrence Berkeley National Laboratory was supported by the US Department of Energy Office of Basic Energy Sciences, Division of Chemical Sciences Contract No. DE-AC02-05CH11231. Work at University of California, Davis was supported by US Department of Energy Office of Basic Energy Sciences, Division of Chemical Sciences Grant No. DESC0007182.

- 
- [1] O. E. Alon, A. I. Streltsov, and L. S. Cederbaum, *J. Chem. Phys.* **127**, 154103 (2007).
  - [2] O. E. Alon, A. I. Streltsov, and L. S. Cederbaum, *Phys. Rev. A* **79**, 022503 (2009).
  - [3] M. Kitzler, J. Zanghellini, C. Jungreuthmayer, M. Smits, A. Scrinzi, and T. Brabec, *Phys. Rev. A* **70**, 041401 (2004).
  - [4] J. Caillat, J. Zanghellini, M. Kitzler, O. Koch, W. Kreuzer, and A. Scrinzi, *Phys. Rev. A* **71**, 012712 (2005).
  - [5] T. Kato and H. Kono, *Chem. Phys. Lett.* **392**, 533 (2004).
  - [6] T. Kato and K. Yamanouchi, *J. Chem. Phys.* **131**, 164118 (2009).
  - [7] T. Kato and H. Kono, *J. Chem. Phys.* **128**, 184102 (2008).
  - [8] T. Kato and H. Kono, *Chem. Phys.* **366**, 46 (2009).
  - [9] T. Kato, H. Kono, M. Kanno, Y. Fujimura, and K. Yamanouchi, *Laser Phys.* **19**, 1712 (2009).
  - [10] M. Nest, T. Klamroth, and P. Saalfrank, *J. Chem. Phys.* **122**, 124102 (2005).
  - [11] M. Nest, *Phys. Rev. A* **73**, 023613 (2006).
  - [12] M. Nest, R. Padmanaban, and P. Saalfrank, *J. Chem. Phys.* **126**, 214106 (2007).
  - [13] M. Nest, *Chem. Phys. Lett.* **472**, 171 (2009).
  - [14] M. Nest, F. Remacle, and R. D. Levine, *New J. Phys.* **10**, 025019 (2008).

- [15] I. S. Ulusoy and M. Nest, *J. Chem. Phys.* **136**, 054112 (2012).
- [16] D. Hochstuhl and M. Bonitz, *J. Chem. Phys.* **134**, 084106 (2011).
- [17] R. P. Miranda, A. J. Fisher, L. Stella, and A. P. Horsfield, *J. Chem. Phys.* **134**, 244101 (2011).
- [18] R. P. Miranda, A. J. Fisher, L. Stella, and A. P. Horsfield, *J. Chem. Phys.* **134**, 244102 (2011).
- [19] G. A. Worth, M. H. Beck, A. Jäckle, and H.-D. Meyer, The MCTDH Package, Version 8.2, 2000. See <http://www.pci.uni-heidelberg.de/tc/usr/mctdh/>
- [20] M. H. Beck, A. Jäckle, G. A. Worth, and H.-D. Meyer, *Phys. Rep.* **324**, 1 (2000).
- [21] G. A. Worth, H.-D. Meyer, and L. S. Cederbaum, *J. Chem. Phys.* **109**, 3518 (1998).
- [22] A. Raab, G. Worth, H.-D. Meyer, and L. S. Cederbaum, *J. Chem. Phys.* **110**, 936 (1999).
- [23] O. Vendrell, F. Gatti, D. Lauvergnat, and H.-D. Meyer, *J. Chem. Phys.* **127**, 184302 (2007).
- [24] O. Vendrell, F. Gatti, and H.-D. Meyer, *J. Chem. Phys.* **127**, 184303 (2007).
- [25] O. Vendrell, F. Gatti, and H.-D. Meyer, *Angew. Chem.* **46**, 6918 (2007).
- [26] M. D. Coutinho-Neto, A. Viel, and U. Manthe, *J. Chem. Phys.* **121**, 9207 (2004).
- [27] T. Hammer and U. Manthe, *J. Chem. Phys.* **134**, 224305 (2011).
- [28] T. Hammer and U. Manthe, *J. Chem. Phys.* **136**, 054105 (2012).
- [29] S. Kvaal, *Phys. Rev. A* **84**, 022512 (2011).
- [30] O. E. Alon, A. I. Streltsov, and L. S. Cederbaum, *Phys. Rev. A* **77**, 033613 (2008).
- [31] U. Manthe, H.-D. Meyer, and L. S. Cederbaum, *J. Chem. Phys.* **97**, 3199 (1992).
- [32] D. J. Haxton, K. V. Lawler, and C. W. McCurdy, *Phys. Rev. A* **83**, 063416 (2011).
- [33] J. Aguilar and J. M. Combes, *Commun. Math. Phys.* **22**, 269 (1971).
- [34] E. Balslev and J. M. Combes, *Commun. Math. Phys.* **22**, 280 (1971).
- [35] N. Moiseyev, P. R. Certain, and F. Weinhold, *Mol. Phys.* **36**, 1613 (1978).
- [36] N. Moiseyev and J. O. Hirschfelder, *J. Chem. Phys.* **88**, 1063 (1987).
- [37] N. Lipkin, R. Lefebvre, and N. Moiseyev, *Phys. Rev. A* **45**, 4553 (1992).
- [38] N. Moiseyev, *Phys. Rep.* **302**, 211 (1998).
- [39] A. S. Dickinson and P. R. Certain, *J. Chem. Phys.* **49**, 4209 (1968).
- [40] J. C. Light, I. P. Hamilton, and J. V. Lill, *J. Chem. Phys.* **82**, 1400 (1985).
- [41] G. C. Corey and D. Lemoine, *J. Chem. Phys.* **97**, 4115 (1992).
- [42] T. N. Rescigno and C. W. McCurdy, *Phys. Rev. A* **62**, 032706 (2000).
- [43] L. Tao, C. W. McCurdy, and T. N. Rescigno, *Phys. Rev. A* **79**, 012719 (2009).
- [44] W. Kohn, *Phys. Rev.* **74**, 1763 (1948).
- [45] T. N. Rescigno, C. W. McCurdy, A. E. Orel, and B. H. L. III, in *Computational Methods for Electron-Molecule Collisions*, edited by W. M. Huo and F. A. Gianturco (Plenum, New York, 1995).
- [46] T. N. Rescigno, B. H. L. III, and C. W. McCurdy, in *Modern Electronic Structure Theory*, edited by D. R. Yarkony (World Scientific, Singapore, 1995), Vol. 1, pp. 501–588.
- [47] A. Jäckle and H.-D. Meyer, *J. Chem. Phys.* **105**, 6778 (1996).
- [48] P. L. Altick, *Phys. Rev.* **169**, 21 (1968).
- [49] J. Dubau and J. Wells, *J. Phys. B* **6**, L31 (1973).
- [50] M. Y. Amusia, N. A. Cherepkov, D. Zivanovic, and V. Radojevic, *Phys. Rev. A* **13**, 1466 (1976).
- [51] W. R. Johnson and C. D. Lin, *J. Phys. B* **10**, L331 (1977).
- [52] C. M. Lee and W. R. Johnson, *Phys. Rev. A* **22**, 979 (1980).
- [53] C. H. Greene, *Phys. Rev. A* **23**, 661 (1981).
- [54] C. D. Lin, *J. Phys. B* **16**, 723 (1983).
- [55] V. Radojevic and W. R. Johnson, *Phys. Rev. A* **31**, 2991 (1985).
- [56] P. F. O'Mahony and C. H. Greene, *Phys. Rev. A* **31**, 250 (1985).
- [57] R. Moccia and P. Spizzo, *Phys. Rev. A* **39**, 3855 (1989).
- [58] J. A. Tully, M. J. Seaton, and K. A. Berrington, *J. Phys. B* **23**, 3811 (1990).
- [59] H.-C. Chi, K.-N. Huang, and K. T. Cheng, *Phys. Rev. A* **43**, 2542 (1991).
- [60] H.-C. Chi and K.-N. Huang, *Phys. Rev. A* **43**, 4742 (1991).
- [61] B. Zhou and C. D. Lin, *Phys. Rev. A* **51**, 1286 (1995).
- [62] D.-S. Kim, S. S. Tayal, H.-L. Zhou, and S. T. Manson, *Phys. Rev. A* **61**, 062701 (2000).
- [63] J.-T. Hsiao, L.-R. Wang, H.-L. Sun, S.-F. Lin, C.-L. Lu, and K.-N. Huang, *Phys. Rev. A* **78**, 013411 (2008).
- [64] R. Wehlitz, D. Lukić, and J. B. Bluett, *Phys. Rev. A* **68**, 052708 (2003).
- [65] R. Wehlitz, D. Lukić, and J. B. Bluett, *Phys. Rev. A* **71**, 012707 (2005).
- [66] P. Olalde-Velasco, E. Méndez-Martínez, J. Jiménez-Mier, R. Wehlitz, and S. B. Whitfield, *Phys. Rev. A* **76**, 032701 (2007).
- [67] L. VoKy, H. E. Saraph, W. Eissner, Z. W. Liu, and H. P. Kelly, *Phys. Rev. A* **46**, 3945 (1992).
- [68] F. Bely-Dubau, J. Dubau, and D. Petrini, *J. Phys. B* **10**, 1613 (1977).
- [69] H. P. Saha and C. D. Caldwell, *Phys. Rev. A* **40**, 7020 (1989).
- [70] M. Kutzner, D. Winn, and S. Mattingly, *Phys. Rev. A* **48**, 404 (1993).
- [71] E. Dias, H. S. Chakraborty, P. C. Deshmukh, and S. T. Manson, *J. Phys. B* **32**, 3383 (1999).
- [72] E. Jannitti, P. Nicolosi, G. Tondello, Z. Yongzhen, and M. Mazzoni, *Opt. Commun.* **63**, 37 (1987).
- [73] M. O. Krause and C. D. Caldwell, *Phys. Rev. Lett.* **59**, 2736 (1987).
- [74] F. Yoshida, L. Matsuoka, R. Takashima, T. Nagata, Y. Azuma, S. Obara, F. Koike, and S. Hasegawa, *Phys. Rev. A* **73**, 062709 (2006).
- [75] NIST atomic spectral database, URL <http://www.nist.gov/pml/data/asd.cfm>
- [76] H. Lin, C.-S. Hsue, and K. T. Chung, *Phys. Rev. A* **65**, 032706 (2002).
- [77] C. D. Caldwell, M. G. Flemming, M. O. Krause, P. van der Meulen, C. Pan, and A. F. Starace, *Phys. Rev. A* **41**, 542 (1990).
- [78] M. Jungen, *J. Chem. Phys.* **74**, 750 (1981).
- [79] J. T. H. Dunning, *J. Chem. Phys.* **90**, 1007 (1989).
- [80] H. Lischka, R. Shepard, F. B. Brown, and I. Shavitt, *Int. J. Quantum Chem. Quantum Chem. Symp.* **15**, 91 (1981).
- [81] R. Shepard, I. Shavitt, R. M. Pitzer, D. C. Comeau, M. Pepper, H. Lischka, P. G. Szalay, R. Ahlrichs, F. B. Brown, and J. Zhao, *Int. J. Quantum Chem. Quantum Chem. Symp.* **22**, 149 (1988).
- [82] H. Lischka, R. Shepard, R. M. Pitzer, I. Shavitt, M. Dallos, T. Müller, P. G. Szalay, M. Seth, G. S. Kedziora, S. Yabushita, and Z. Y. Zhang, *Phys. Chem. Chem. Phys.* **3**, 664 (2001).

- [83] H. Lischka, T. Müller, P. G. Szalay, I. Shavitt, R. M. Pitzer, and R. Shepard, *WIREs Comput. Mol. Sci.* **1**, 191 (2011).
- [84] H. Lischka *et al.*, COLUMBUS, an *ab initio* electronic structure program, 2012, release 7.0.
- [85] M. Stener, G. Fronzoni, D. Toffoli, and P. Decleva, *Chem. Phys.* **272**, 337 (2002).
- [86] J. Zobeley, L. S. Cederbaum, and F. Tarantelli, *J. Chem. Phys.* **108**, 9737 (1998).
- [87] W. V. Niessen, L. S. Cederbaum, W. Domcke, and G. H. F. Diercks, *Chem. Phys.* **56**, 43 (1981).
- [88] A. J. Yench, M. C. A. Lopes, M. A. MacDonald, and G. C. King, *Chem. Phys. Lett.* **310**, 433 (1999).
- [89] C. E. Brion and J. P. Thomson, *J. Electron Spectrosc. Relat. Phenom.* **33**, 301 (1984).
- [90] R. Whitehead, *Nucl. Phys. A* **182**, 290 (1972).
- [91] A. I. Streltsov, O. E. Alon, and L. S. Cederbaum, *Phys. Rev. A* **81**, 022124 (2010).
- [92] A. I. Streltsov, K. Sakmann, O. E. Alon, and L. S. Cederbaum, *Phys. Rev. A* **83**, 043604 (2011).
- [93] O. E. Alon, A. I. Streltsov, K. Sakmann, A. U. J. Lode, J. Grond, and L. Cederbaum, *Chem. Phys.* **401**, 2 (2012).